Rheological and Antimicrobial Properties of Silica and silver Nanoparticles-reinforced K-carrageenan/hydroxyethyl Cellulose Composites for Food Packaging Applications

Balasubramanian Rukmanikrishnan (rukmibala@gmail.com)
Yeungnam University https://orcid.org/0000-0001-6207-7271

Srinivasan Ramalingam
Yeungnam University

Sam Soo Kim
Yeungnam University

Jaewoong Lee
Yeungnam University

Research Article

Keywords: Hydroxyethyl cellulose, k-carrageenan, silica, silver, rheology, antimicrobial properties

Posted Date: February 23rd, 2021

DOI: https://doi.org/10.21203/rs.3.rs-223398/v1

Version of Record: A version of this preprint was published at Cellulose on April 17th, 2021. See the published version at https://doi.org/10.1007/s10570-021-03873-z.

Abstract

Sustainable food packaging films were developed using a combination of k-Carrageenan (C), hydroxyl ethyl cellulose (H), silicon dioxide (SiO_2), and silver (Ag) nanoparticles. The CH-SiO_2/Ag nanocomposites showed promising results, mainly due to their transparency, flexibility, low cost, and environmental friendliness. The structure and uniform morphology of the CH-SiO_2/Ag nanocomposites were determined by FT-IR, XRD, and SEM analysis. Barrier properties (water vapor permeability-WVP), thermal properties ($T_{5\%}$ loss, char yield), and mechanical properties determined for the CH and CH-SiO_2/Ag nanocomposites, which improved by 3.3–1.9 $\times 10^{-9}$gm/m^2 Pas (WVP), 59.1-115.7 ^oC ($T_{5\%}$), 13.4–29.3 % (char yield), 23.8–41.5 MPa(tensile strength), and 22.3–28.9 (EB), respectively. The contact angles of the CH-SiO_2/Ag nanocomposites were in the range of 60.1–76.4. The UV transmittance of the CH composites decreased with the addition of SiO_2 and Ag nanoparticles. However, the transparency of the composites was not affected, and it inhibited UVA and UVB rays by the addition of Ag nanoparticles.

The viscosity of the CH composites increased with the SiO2 content and decreased with the shear rate. All the composites exhibited shear-thinning behavior. The storage modulus of the prepared composites is higher than the loss modulus in the entire frequency region. Overall, SiO_2 and Ag nanoparticles improved the hydrophilic nature of the CH-SiO_2/Ag films and showed significant activity against six common food pathogens, *Staphylococcus aureus, Bacillus cereus, Listeria monocytogenes, Bacillus subtilis, Salmonella typhi, and Cronobacter sakazakii*. The synergistic combination of CH-SiO_2/Ag nanocomposite has potential for packaging and other biomedical applications.

Introduction

These days there is a great attention on the terms environment friendly, green synthesis, sustainable, biocompatible and biodegradable, in the area of material science research. Particularly, in polymers and plastics being used in many sectors for packaging (Castro-Mayorga et al. 2016; Gholam et al. 2013; Yoldas et al. 2014; Tippabattini et al. 2013). However, it is damaging our ecosystem, human and animal health, due to unrealizable utilization (Zhili et al. 2017; Rhim et al. 2014). Owing to the above concerns, biopolymer-based composites are an immediate alternative with reasonable parameters such as low cost, biodegradability, biocompatibility, and low toxicity, and are available from sustainable natural resources.

Carrageenan is a linear and high molecular weight biopolymer derived from red seaweed (*Eucheuma spinosum*) and is available in different structures such as kappa, iota, and alpha carrageenan. It was classified based on the composition of 3, 6 –anhydro-galactose and ester sulfate groups. Kappa-carrageenan contains the lowest content of sulfate ester groups, which has better film-forming ability than others. Carrageenan is used in many foods and cosmetic and pharmaceutical applications (Yunpeng et al. 2019; Zineb et al. 2019; Bianca-Ioana et al. 2020; Afsaneh et al. 2018; Maria et al. 2010; Joana et al. 2013; Hou et al. 2019).

Hydroxyethyl cellulose is the most important non-ionic water-soluble cellulose derivative. It is a biodegradable material that is widely used in food, coating, medicine, and papermaking industries (Zhili et al. 2017).

However, both k-Carrageenan and hydroxyethyl cellulose are mechanically weak and have poor barrier properties (Mithilesh et al. 2019; Cristina et al 2010; Márcia et al. 2012; Jéssica de et al. 2020; Andong et al. 2013).

To overcome these disadvantages, the incorporation of two more biopolymers and the addition of inorganic additives is the best method (Lokesh et al 2014; Maria et al. 2010). The above disadvantages are easily overcome by the preparation of two or more biopolymers based on the addition of inorganic additives such as TiO_2, ZnO, GO, MTT clay, SiO_2, and Ag nanoparticles (Ivan et al. 2020; Rhim 2013; Izabela et al. 2008; Guanzheng et al. 2019). Silica has attracted great attention because of its chemical inertness, morphology, availability, low cost, easy surface functionalization, and well-defined particle size (Merve et al. 2019). Silica nanoparticles have been used in various applications such as drug delivery systems, absorbents for bioactive compounds, molecular imaging, sensors, and optical devices (Iñigo et al. 2018). On the other hand, the reinforcement of Ag nanoparticle-based polymer composites help to develop active packaging materials. The antimicrobial properties of the Ag nanoparticles improve or maintain the self-life, safety, and quality of the food product (Castro-Mayorga et al. 2016; Márcia et al. 2012; Li et al. 2011; Mahdieh et al. 2018). Both the synergistic combination of Ag and SiO_2 nanoparticles help to develop active materials with improved barrier, mechanical, thermal, and antimicrobial properties of the polymer composites.

In this work, we prepared a synergistic composition based on k-carrageenan, hydroxyethyl cellulose, Ag, and SiO_2 nanoparticles. We focused and thoroughly studied the rheological properties of the CH-SiO_2/Ag nanocomposites. In addition, the effect of Ag and SiO_2 on the water barrier, contact angle, and mechanical properties were systematically explored.

Materials And Methods

K-Carrageenan (Ash content 40.0% and viscosity min 10.0 in 0.30% in water at 25^o °C), 2-hydroxyethyl cellulose (molecular weight M_v ~ 1,300,000), and SiO_2 (particle size 50 nm, BET) were purchased from Sigma Aldrich, South Korea and used as received. Glycerin, sodium citrate, epichlorohydrin, and citric acid were purchased from Dajang Chemicals, South Korea. A silver colloid (Nanomix-silver 30 000 ppm) was obtained from Meiji Nanotech (Seoul, Korea). All reagents were used as received.

Preparation of CH-SiO_2/Ag nanocomposite films

CH with various concentrations of SiO_2 (0, 2.5, 5, 7.5, and 10 wt%) and Ag nanoparticles were prepared by the solvent evaporation method. First, k-carrageenan (0.5g) and hydroxyethyl cellulose (0.5g) were dispersed in glycerin (3g) to ensure that there was no particle agglomeration. Then, 75 mL of distilled water was added with continuous stirring and the temperature was increased to 80 ^{o}C for 15 min. The crosslinking agent of epichlorohydrin (4 wt%) was added to the above solution. Subsequently, citric acid (0.5g) and sodium citrate (0.5g) were mixed one by one in the reaction mixture at same condition. SiO_2 was dispersed in ethanol separately in sonicated for 60 min at 50 ^{o}C. The dispersed SiO_2 was mixed with the hydrogel reaction mixture and continuously stirred for another 60 min. The temperature was reduced to 50 ^{o}C and 0.25 mL of silver

colloid solution was added with vigorous stirring. Finally, the CH-SiO_2/Ag nanocomposite hydrogel was spread on the glass plate and dried at ambient temperature, and then removed from the glass plate, under dried conditions. Similarly, the same procedure was followed for all the (a) CH (b) CH-SiO_2-2.5 wt% (c) CH-SiO_2-5 wt % (d) CH-SiO_2-7.5 wt% (e) CH-SiO_2-10 wt% (f) CH-SiO_2-10 wt% /Ag nanocomposite preparations.

Result And Discussion

FT-IR

The FT-IR spectra of the CH-Ag composites are shown in Fig. 1. The characteristic absorption peaks at 2961, 2865 (CH stretching), 3349 (O-H stretching), 1222 (O = S = O asymmetric), 918 (C-O-C stretching), and 843 (0-SO3 stretching vib of β-D-galactose). The C-O of 3, 6-anhydro-D-galactose and C-O-SO_3 of D-galactose-4-sulfate presence in k-carrageenan exhibited characteristics at 922 and 846 cm^{-1}. A broad band at 3356 and 1404 attributed to, or belongs to the OH stretching vibration and OH bending vibration of hydroxylethyl cellulose. The aliphatic C-H stretching, C-O-C stretching vibration, and C-O stretching vibration are represented at 2876, 1036, 1010, and 1108 cm^{-1}, respectively (Zhili et al. 2017; Márcia et al. 2012; Li et al. 2011). In the spectrum of $CHSiO_2$ nanocomposites in the region of 800–1200 cm^{-1}, shoulder peaks appear at 899 cm^{-1} (Si-OH) (Cristina et al. 2010). In addition, there are two absorption bands around 900–1100 cm^{-1} due to the stretching vibration of Si-O-Si and Si-O-C bonds, whose intensity increases upon increasing the SiO_2 content (Joana et al. 2013; Bo et al. 2018). The absorption near 1062 cm^{-1}, 965 cm^{-1}, and 792 cm^{-1} were attributed to the asymmetric stretching vibration, symmetric stretching vibration, and bending vibration of Si-O-Si, respectively. This indicates the intermolecular interactions between the components in the CH-SiO_2 nanocomposites.

XRD

The XRD patterns of CH and CH-SiO_2/Ag composites are shown in Fig. 2. The broad and clear diffraction peaks appeared at 23.1° for the CH composites, indicating the amorphous structure of the composites. Further, w by the addition or increasing content of SiO_2 nanoparticles, this peak shifted slightly, and the intensity of the peak for the CH-SiO_2-10 wt% composites increased. The XRD patterns of the CH-SiO_2-10 wt% /Ag nanocomposites all the materials dispersed well, and the amorphous structure of k-C was not affected and altered by the incorporation of HEC, SiO_2, and Ag nanoparticles.

UV

UV-VIS spectroscopy is a very important technique for studying the transmittance and absorption of food packaging composite films. Figure 3 and Table 1 show that the transmittance of the CH and CH-SiO_2-10 wt% /Ag nanocomposites are in the ranges of 92.2–89.7 and 91.5–89.5 % at 800 nm and 600 nm, respectively. There was no significant reduction in their transmittance. However, at 280 nm, the transmittance decreased to 71.7–56.6 % for CH and CH-SiO_2-10 wt% /Ag composites, respectively. The transmittance of the CH composites decreased from 800 to 280 nm from 92.2% to 71.7 %, and for the CH-SiO_2-10 wt% composite is 90.7% to 64.1 %. The addition of SiO_2 nanoparticles gradually decreased the transmittance, but the addition of

Ag decreased the transmittance by 56.6 %, at 280 nm. Both these nanoparticles improved the light barrier properties of the CH composites and blocked UV light transmission. The thermal, mechanical, and FT-IR results support the uniform dispersion of SiO_2 and Ag nanoparticles. CH-SiO_2-10 wt% /Ag nanocomposites are the perfect composition for food oxidative deterioration (Hou et al. 2019; Mahdieh et al. 2018). The color parameter is very important in packaging films and is affected by the addition of SiO_2 and Ag nanoparticles. The lightness (L), redness (a), and yellowness (b) of the CH composites were not significantly affected by the addition of SiO_2 nanoparticles. But the CH-SiO_2/Ag nanocomposites color values reduced significantly. The above results indicate that the CH-SiO_2/Ag nanocomposites have the highest UV barrier property, without significant sacrifice to the transparency of the neat CH composite films.

Table 1
UV-transmittance, thickness, and color values of CH and CH-SiO2/Ag nanocomposite films.

Sample	Thickness (mm)	T (%) at 600 nm	Lightless (L*)	Redness (a*)	Yellowness (b*)	Water vapor permeability ($\times10^{-9}$gm/m^2 Pas)	Water contact angle (º)
CH	0.04	91.5	85.87	1.22	-3.13	3.3	60.1
CH-SiO_2-2.5 wt%	0.04	91.0	85.72	1.18	-2.96	3.1	63.5
CH-SiO_2-5 wt%	0.05	90.7	85.66	1.16	-2.95	2.7	68.2
CH-SiO_2-7.5 wt%	0.05	90.5	85.18	1.16	-2.86	2.5	70.5
CH-SiO_2-10 wt%	0.05	90.3	84.73	1.14	-2.84	2.1	73.6
CH-SiO_2-10 wt%/Ag	0.05	89.5	83.04	1.09	-1.77	1.9	76.4

WVP

Generally, biopolymers are highly sensitive to moisture, which restricts their application in several fields. To overcome these disadvantages, preparing nanocomposites or incorporating hydrophobic additives is the best solution. This restricted the water molecules to cross the nanocomposite films and decreased the WVP values. The prepared CHSA nanocomposites are shown in Table 1. The WVP values of CH composites 3.3 $\times10^{-9}$gm/m^2 Pas, which reduced to 3.1, 2.7, 2.5 and 2.1 $\times10^{-9}$gm/m^2 Pas, by the addition of 2.5, 5, 7.5, 10 wt % of SiO_2 nanoparticles respectively and it further reduced to 1.9 $\times10^{-9}$gm/m^2 Pas by the addition of Ag nanoparticles respectively. This improvement is mainly due to the fact that the HEC is slightly more crystalline than k-C, and it restricts k-C to swell in water upon reinforcement. The reinforcement effect of HEC restricted the k-C materials to swell in water because HEC is slightly more crystalline than k-C (Mithilesh et al. 2019). The improvement or reduction in WVP value is mainly due to the hydrophobic nature of SiO_2 nanoparticles, homogeneously dispersed in the CH matrix, and it also provided strong intermolecular interactions between or

with the polymer matrix (Jéssica de et al. 2020). Furthermore, Ag nanoparticles reduced the intermolecular spacing within the CHS nanocomposites, thus significantly reducing their WVP values (Márcia et al. 2012).

CA

Surface hydrophilic/hydrophobic properties and wettability are interesting and important parameters for polymer composite films measured by CA. The CA of the CH and CH-SiO2-10 wt% /Ag nanocomposite films is shown in Table 1. The CA of neat CH composite film is 60.1, then it increased significantly to 63.5, 68.2, 70.5 and 73.6^{o} CH-SiO_2-2.5 wt%, CH-SiO_2-5 wt %, CH-SiO_2-7.5 wt%, and CH-SiO_2-10 wt% nanocomposites respectively. It further increased (76.4^{o}) upon incorporation of Ag nanoparticles. This is mainly attributed to the surface cohesiveness and interaction between the components.

TGA

The rate of decomposition and thermal stability of the CH and CH-SiO2-10 wt% /Ag nanocomposites were studied by TGA under nitrogen atmosphere (Table 2 and Fig. 4). The initial thermal degradation of the CH composites is very low. The 5% gravimetric loss of the CH composites was 59.1 ^{o}C, which increased slowly with increasing the content of SiO_2. The addition of SiO_2 increased the $T_{5\%}$ and $T_{10\%}$ loss values from 69.1-115.7 ^{o}C and 81.1-150.4 ^{o}C, which is nearly 48.9 % ($T_{5\%}$) and 46 % ($T_{10\%}$). The main reason for the significant improvement in the thermal stability of the CH-SiO2-10 wt% /Ag nanocomposites is (mainly due to the) SiO_2 nanoparticles forming continuous protective solid layers, so that oxidation degradation becomes slower. It also increased the char yield of the nanocomposites, which increased by 13.4 % (CH) to 29.3 % (CH-SiO2-10 wt% /Ag). Moreover, incorporation of Ag nanoparticles increased the thermal stability to the next level. It significantly increased $T_{5\%}$ and char yield to 115.7 ^{o}C and 29.3 %, respectively. These results are encouraging for CH-based SiO_2 and Ag composites, and the results are comparable with previously reported nanocomposites (Yunpeng et al. 2019; Mithilesh et al. 2019; Andong et al. 2013; Mahdieh et al. 2018). Overall, the results suggest that the inorganic SiO_2 and Ag nanoparticles are uniformly dispersed and distributed on the polymer surface and stabilize the organic matrices.

DSC

The DSC thermogram is a very important thermal analysis (in polymer nanocomposites) to determine the effect of nanoparticles on the polymer composite structures, such as T_g and T_m (Table 2). The T_g and T_m of the CH composites improved from 146.7 to 149.5 ^{o}C by the incorporation of SiO_2 and Ag particles. These changes were even more pronounced for the CH-SiO_2-10 wt% /Ag composites, which showed higher T_g and T_m values. The dispersion of SiO_2 disturbs the T_g and T_m of polymer composites by hydrogen bonding interactions between the polymer chains. This formation of bonds reduces the segmental mobility in the polymer chain and hence increases T_g [28]. This result is consistent with the TGA and mechanical properties of the CH-SiO_2-10 wt% /Ag composites (Castro-Mayorga et al. 2016; Jéssica de et al. 2020; Lokesh et al. 2014; Mahdieh et al. 2018).

SEM

SEM micrographs of CH and CH-SiO_2-10 wt% /Ag nanocomposites are shown in Fig. 5. The neat CH composites exhibited a smooth, uniform structure, suggesting compatibility and dispersion of k-C and HEC polymers when increasing the SiO_2 nanoparticles in the CH composites. There are no structural changes at low concentrations of SiO_2, but at high concentrations, it is very slightly agglomerated on the surface, without any cracks. The roughness of the CH surface was slightly enhanced by the addition of SiO_2 (10 wt %). In the CH-SiO_2-10 wt% /Ag nanocomposites, the Ag nanoparticles were not observed in the SEM images, even in the cross-section images. The smooth and homogeneous cross section of the prepared composites was not affected by the inorganic SiO_2 and Ag nanoparticles (Castro-Mayorga et al. 2016; Joana et al. 2013; Jéssica de et al. 2020; Maria et al. 2010; Mahdieh et al. 2018). The EDX analysis of CH-SiO_2-10 wt% /Ag reveals the presence of elements such as C, O, Na, and Cl along with Si and Ag in the CH-SiO_2 composites. These data confirm the homogenous distribution of C, O, Si, S and Ag in CH-SiO_2-10 wt% /Ag nanocomposites and displays a well-defined compositional profile of the hybrid.

Mechanical properties

CH with SiO_2 and Ag nanocomposites were measured for tensile strength (TS) and elongation at break (EB) to evaluate the effect of SiO_2 and Ag nanoparticles. TS and EB (Table 2) were evaluated for the effect of SiO_2 and Ag nanoparticles on the CH composites. The TS of neat CH composites increased gradually and reached the highest value of 41.5 MPa for the CH-SiO_2-10 wt% /Ag nanocomposites. It almost improved by 42.6 % of TS. Initially, the TS values of the CH-SiO_2-2.5 wt% nanocomposites were slightly higher than those of the CH composites. Then, SiO_2 increased to 5 wt% (CH-SiO_2-5 wt%) to 29.5 MPa. The CH-SiO_2-10 wt% nanocomposites were also significantly higher than those of the CH-SiO_2-7.5 wt% nanocomposites. However, the same concentration of SiO_2 with Ag nanocomposites demonstrated superior TS values (41.5 MPa). The observed improvement in the TS is mainly due to the reinforcement effect of homogeneously dispersed inorganic nanoparticles and intermolecular adhesion and interaction between the polymers and SiO_2 and Ag inorganic nanoparticles [15]. The EB of CH and CH-SiO_2-10 wt% /Ag nanocomposites are in the range of 22.3–28.9 %. At low concentrations of SiO_2, EB increased drastically, but at high concentrations, it improved or increased slightly to higher values. By the addition of Ag nanoparticles, it improved from 27.5% to 28.9 %. This may be due to the greater interaction between CH and SiO_2/Ag nanoparticles. The extreme rigidity of these composites restrict their EB to a considerable extent (Afsaneh et al. 2018; Cristina et al. 2010; Maria et al. 2010; Mahdieh et al. 2018).

Table 2
Thermal, mechanical, water vapor permeability, and contact angle properties of the CH and CH-SiO2/Ag nanocomposite films.

Sample	TGA			DSC		Tensile strength (MPa)	Elongation at break (%)
	$T_{5\%}$	$T_{10\%}$	CY (%)	T_g (°C)	T_m (°C)		
CH	59.1	81.1	13.4	146.7	221.5	23.8	22.3
CH-SiO_2-2.5	69.1	91.5	19.1	146.5	222.1	26.2	23.5
CH-SiO_2-5	83.9	102.7	24.0	147.4	222.6	29.5	24.8
CH-SiO_2-7.5	94.7	129.5	26.1	148.2	223.3	33.2	26.4
CH-SiO_2-10	107.3	142.1	26.7	148.9	225.7	37.1	27.5
CH-SiO_2-10/Ag	115.7	150.4	29.3	149.5	2264	41.5	28.9

Rheology

The storage modulus (G') and loss modulus (G') were studied for the 3D structure and coordination bonds between k-C, HEC, SiO_2, and Ag nanocomposites. G' and G" of CH-SiO_2-10 wt% /Ag nanocomposites are characterized in the form of angular frequency (0–100 rad/s), as shown in Figs. 6 and 7. The G' increased and G" decreased continuously with increasing frequency. G' is almost independent of the entire frequency range. At high frequencies, G" is dependent on the frequency. Both the addition of SiO_2 and Ag nanoparticles significantly improved on G' and G". The continuous increase in G' from low to high frequency is mainly due to the interaction and concentration of SiO_2 and Ag nanoparticles. It improved the fine structure and gelling network (Pinheiro et al. 2011).
However, the rate of increase of G' shows that the elastic properties of the gelling hydrogel dominate. Figure 7 shows the loss modulus of the CH composites. It was observed as very steep in the low frequency region. When the frequency is increased, it minimizes the slippage level and maintains a reasonable level. In the high-frequency region (20–100 rad/s), G" increased, which indicated that the nanocomposites exhibited a more elastic behavior for the materials. The concentrations of SiO_2 and Ag played an important role in the G' and G" of the CH composites.

The complex viscosity versus frequency of the CH and CH-SiO_2-10 wt% /Ag nanocomposites is shown in Fig. 8. The nanocomposites exhibited shear-thinning behavior. The molecular entanglements and the interactions disrupt at or up to certain initial or low angular frequencies. The addition of SiO_2 increased the sensitivity and increased the complex viscosity even at low concentrations of SiO_2 nanoparticles. These results suggest that a significant amount of SiO_2 and Ag nanoparticles diffused into the polymer interlayers.

From the dynamic viscoelastic results of G’ and G’ and the complex viscosity of CH and CH-SiO_2-10 wt% /Ag nanocomposites showed strong interactions between CH and SiO_2 and Ag nanoparticles.

Figure S4 shows the shear dependent viscosity results for the CH-SiO_2-10 wt% /Ag nanocomposites. The viscosity of the CH composites decreased at a low shear rate. This shear thinning or non-Newtonian behavior of composites is due to the molecular disentanglements in their structure and aligned with the flow direction (Hadi et al. 2020).

The viscosity of the CH composites was 51.2 Pas, which increased to 261.0 Pas by the addition of 10 wt% of SiO_2 nanoparticles at a 1/s shear rate (Fig. 9). The highest viscosity of the CH-SiO_2-10 wt% composites was further improved by the Ag nanoparticles. CH-SiO_2-10 wt% /Ag exhibited the maximum viscosity in the low-and high-viscosity regions. These results are attributed to the structural characteristics such as size, confirmation, rigidity, and interaction with different concentrations of SiO_2 and Ag particles. The CH-SiO_2-10 wt% /Ag nanocomposites exhibited high viscosity over the whole shear range as the structure of SiO_2/Ag embedded in a continuous matrix on the CH following the deformable fillers in a viscous entangled network, resulting in higher viscosities (Xudong et al. 2017).

At low shear rates, the viscosity of the nanocomposite is higher than that of neat CH, but the high shear rate decreases significantly. This may be attributed to the coalescence of nanoparticles, which leads to a decrease in the surface area and interaction between the nanoparticles and polymer matrices.

The full range of shear stress versus shear rate of CH and CH-SiO_2-10 wt% /Ag composites is shown in Fig. 10. The flow properties of the nanocomposites were also described. Similarly, the shear stress increased with increasing the shear rate and concentration of SiO_2 and Ag nanoparticles. The neat CH composites showed the lowest shear stress, which may be due to the absence of large attractive forces among the k-C and HEC components. The addition of SiO_2/Ag nanoparticles had a positive influence on the viscosity and shear stress of the CH composites. Similar flow and viscosity behaviors of the composites have already been reported. The effect of SiO_2 and Ag nanoparticles is more pronounced at low shear rates, and it (or the relative effect) diminishes with increasing shear rates due to shear thinning. Moreover, the trend of the viscosity and shear stress with shear rate is very similar to the reported composites.

Antimicrobial properties

The antimicrobial properties of the CH and CH-SiO_2-10 wt% /Ag nanocomposites were studied by the well diffusion method and the results of their inhibition zone of the CH-SiO_2-10 wt% /Ag nanocomposite films are shown in Table 3. This study was broadly performed using four different gram positive and two different gram-negative pathogens. The neat CH and CH-SiO_2-10 wt% based nanocomposites had no considerable antimicrobial effect on the bacteria. However, the combination or incorporation of Ag nanoparticles exhibited more pronounced antimicrobial activity against both gram-positive and gram-negative bacteria. The CH-SiO_2-10 wt% /Ag nanocomposite showed a high antimicrobial inhibition zone against Staphylococcus aureus (34 mm) and less activity against Bacillus cereus (15.33 mm). However, the clear antimicrobial mechanism of Ag NP is still not clear because it includes several reasons, such as the outer membrane, degradation of

structural changes, and finally death of bacterial cells (Rhim et al. 2014; Paul et al 2005). The addition of Ag NPs greatly improved the antimicrobial properties of CH-SiO_2-10 wt% nanocomposites and extended their potential applications in packaging films.

Table 3
The antimicrobial activities of the CH and CH-SiO2Ag nanocomposite films.

Organism	Zone of growth inhibition (mm)						
	Ciprofloxacin (Control)	CH	CH-SiO_2-2.5	CH-SiO_2-5	CH-SiO_2-7.5	CH-SiO_2-10	CH-SiO_2-10/Ag
Staphylococcus aureus	28.7	N/D	N/D	N/D	N/D	N/D	34.0
Bacillus cereus	26.7	N/D	N/D	N/D	N/D	N/D	15.3
Listeria monocytogenes	22.7	N/D	N/D	N/D	N/D	N/D	19.7
Bacillus subtilis	35.7	N/D	N/D	N/D	N/D	N/D	19.0
Salmonella typhi	33.0	N/D	N/D	N/D	N/D	N/D	22.3
Cronobacter sakazakii	24.7	N/D	N/D	N/D	N/D	N/D	25.7
N/D- Not detected; mm-millimeter.							

Conclusion

Novel synergistic combinations of CH and CH-SiO_2-10 wt% /Ag nanocomposites were prepared successfully and studied well for food packaging applications. FT-IR, XRD, and SEM analyses revealed the structure, morphology, and homogenous dispersion of all the materials. All the composites exhibited shear thinning behavior, and their viscosity increased with increasing polyacrylamide content. The storage modulus of the prepared hydrogel composites was in the range of 815.8-1242.7 at 1 rad/s, and it increased continuously throughout the frequency region. The dynamic rheological properties of AP and AP-QAS hydrogels indicated that the prepared hydrogel composites had good mechanical strength. The addition of SiO_2 and Ag nanoparticles significantly improved the TS and EB of the CH composites. It increased 42.69 % TS and 23 % EB. The UV-transmittance values of the CH composites reduced gradually with increasing SiO_2 and Ag nanoparticles, and these barrier properties are good for food packaging applications. Both inorganic nanoparticles improved the hydrophilic nature of the CH composites, which reduced the WVP values from 3.3 to 1.9 $\times 10^{-9}$ gm/m^2 Pas and increased the CA values from 60.1 ° to 76.4°. From the TGA and DSC results, nanoparticles delayed the thermal degradation of the CH composites. The $T_{5\%}$ are in the range of 59.1-115.7 °C, CY (13.4–29.3 %), T_g (146.7-149.5 °C), and T_m (221.5-226.4 °C), respectively. Finally, the Ag-added CH-SiO_2 nanocomposites showed excellent antimicrobial activity against gram-positive and gram-negative pathogens. These developed CH-SiO_2-10 wt% /Ag nanocomposites are suitable for active food processing in biomedical applications.

Declarations

Conflicts of interest

There are no conflicts to declare.

Funding Sources

The authors declare no competing financial interest.

ACKNOWLEDGMENT

This research was supported by Yeungnam University in the form of a research grant in 2020.

References

1. Afsaneh N, Mohammad TY, Mohammad G, ShaobinW (2018) Biodegradable κ-carrageenan/nanoclay nanocomposite films containing *Rosmarinus officinalis* L. extract for improved strength and antibacterial performance. Int J Biol Macromol 115:227-235.
2. Andong L, Lars AB (2013) Fire-retardant and ductile clay nanopaper biocomposites based on montmorrilonite in matrix of cellulose nanofibers and carboxymethyl cellulose. Eur Polym J 49:940-949.
3. Bianca-Ioana D, Bogdan S, Maria-Cristina P (2020) Synthesis and characterization of κ-carrageenan bio-nanocomposite films reinforced with bentonite nanoclay. Int J Biol Macromol 154:9-17.
4. Bo Y, Christos R, Jianshe C (2018) Extensional and shear rheology of a food hydrocolloid. Food Hydrocolloids 74:296-306.
5. Bruna da SP, Marcela FS, Paulo RSB, Daniela MFO, Edgardo AGP, Ana AWH (2015) Cellophane and filter paper as cellulosic support for silver nanoparticles and its thermal decomposition catalysis. Carbohydr Polym 133:277–283.
6. Castro-Mayorga JL, Fabra, MJ, Lagaron JM (2016) Stabilized nanosilver based antimicrobial poly(3-hydroxybutyrate-co-3-hydroxyvalerate) nanocomposites of interest in active food packaging. Innov Food Sci Emerg 33:524–533.
7. Cristina BS, Roberto JAB, Delilah FW, Tina GW, Tara HM (2010) Composite Edible Films Based on Hydroxypropyl Methylcellulose Reinforced with Microcrystalline Cellulose Nanoparticles. *J Agric Food Chem* 58:3753–3760.
8. Gholam RM, Adeleh A (2013) Synthesis of kappa-carrageenan-g-poly(acrylamide)/ sepiolite nanocomposite hydrogels and adsorption of cationic dye. Polym Bull 70:2451–2470.
9. Guanzheng W, Yanjia G, Xiuliang H, Ruiqing L, Huizhen K, Xueliang X (2019) Hybrid Nanocomposites of Cellulose/Carbon-Nanotubes/Polyurethane with Rapidly Water Sensitive Shape Memory Effect and Strain Sensing Performance. Polymers 11: 1586 (1-14).

10. Hadi HG, Mohammad HE, Mohammadreza K, Paul VM, Seyed MHH (2020) Rheological and interfacial properties of basil seed gum modified with octenyl succinic anhydride. Food Hydrocolloids 101:105489.
11. Hou X, Xue Z, Liu J, Yan M, Xia Y, Ma Z (2019) Characterization and property investigation of novel eco-friendly agar/carrageenan/TiO2 nanocomposite films. J Appl Polym Sci 136:47113 (1 of 12).
12. Iñigo FB, Prospero DP, Reynaldo VS, Blanca GA, Raffaele P (2018) Bioactive mesoporous silica nanocomposite films obtained from native and transglutaminase-crosslinked bitter vetch proteins. Food Hydrocolloids 82:106-115.
13. Ivan K, Alexander Z, Ludmila K, Sabina K, Jiří D (2020) Synergistic effects in Methylcellulose/Hydroxyethylcellulose blend: Influence of components ratio and graphene oxide. Carbohydr Polym236:116077.
14. Izabela B, Piotr W, Tomasz H (2008) Organic–inorganic nanocomposites of (2-hydroxypropyl) cellulose as a precursor of nanocrystalline zinc oxide layers. Polym Adv Technol 19:1860–1867.
15. Jasmina S, Danijela K,ˇZeljka J, Maja VS, Vesna MS, Bojana O (2014) A comprehensive approach to in vitro functional evaluation of Ag/alginate nanocomposite hydrogels. Carbohydr Polym 111:305–314.
16. Jéssica de MF, Germán AV, Lenilton SS, Marta ERD, Carlos EMC, Regina de FPMM, Alcilene RMF (2020) Hydroxypropyl methylcellulose-TiO_2 and gelatin-TiO_2 nanocomposite films: Physicochemical and structural properties. Int J Biol Macromol 151:944-956.
17. Joana TM, Ana IB, Ana CP, Bartolomeu WSS, Miguel AC, Bartolomeu WSS, Miguel AC, António AV (2013) Biocomposite Films Based on κ-Carrageenan/Locust Bean Gum Blends and Clays: Physical and Antimicrobial Properties. Food Bioprocess Technol 6:2081–2092.
18. Levente C, Dusan KB, Veronika N, Suzana DB, Adriaan SL, George G, Vladimir D (2012) Viscoelastic properties and antimicrobial activity of cellulose fiber sheets impregnated with Ag nanoparticles. Carbohydr Polym 90:1139– 1146.
19. Li SM, Ning J, Ma MG, Zhe Z, Liu QH, Sun RC (2011) Cellulose–silver nanocomposites: Microwave-assisted synthesis, characterization, their thermal stability, and antimicrobial property. Carbohydr Polym 86:441-447.
20. Lokesh RR, Niranjan RS, Pravin GK, Shashank TM (2014) Preparation and Characterization of K-Carrageenan/Nanosilica Biocomposite Film. J Mat 2014: 736271 (1-8).
21. Mahdieh S, Mahmod SK, Reza RM, Babak G, Hossein SK (2018) Development and evaluation of chitosan based active nanocomposite films containing bacterial cellulose nanocrystals and silver nanoparticles. Food Hydrocolloids 84:414-423.
22. Maria DSG, Loic H, José ML (2010) Morphology and Water Barrier Properties of Nanobiocomposites of κ/ι-Hybrid Carrageenan and Cellulose Nanowhiskers. *J Agric Food Chem* 58, 24:12847–12857.
23. Márcia RM, Luiz HCM, Valtencir Z (2012) Development of cellulose-based bactericidal nanocomposites containing silver nanoparticles and their use as active food packaging. J Food Eng 109:520-524.
24. Maria DSG, Loic H, Jose ML (2010) Nanobiocomposites of Carrageenan, Zein, and Mica of Interest in Food Packaging and Coating Applications. J Agric Food Chem 58: 6884–6894.
25. Merve Y, Huseyin AO, Yilmaz MD (2019) Transition Metal Chelated Biopolymer Coated Mesoporous Silica Nanoparticles as Highly Efficient, Stable, and Recyclable Nanocatalysts for Catalytic Bleaching. *Chem*

Select 4:2084 –2088.

26. Mithilesh Y, Chiu FC (2019) Cellulose nanocrystals reinforced κ-carrageenan based UV resistant transparent bionanocomposite films for sustainable packaging applications. Carbohydr Polym 211:181-194.
27. Paul P, Stephen P, Rouillard JM, Zhengfei Z, Jaebeom L, LeeJW, Erdogan G, Nicholas AK (2005) Layer-by-Layer Assembly of Nacre-like Nanostructured Composites with Antimicrobial Properties. Langmuir 21:11915-11921.
28. Pinheiro AC, Bourbon AI, Rocha C, Ribeiro C, Maia JM, Goncalves MP, Teixeira JA, Vicente AA (2011) Rheological characterization of k-carrageenan/galactomannan and xanthan/galactomannan gels: Comparison of galactomannans from non-traditional sources with conventional galactomannans. Carbohydr Polym 83:392–399.
29. Rhim JW, Wang LF (2014) Preparation and characterization of carrageenan-based nanocomposite films reinforced with clay mineral and silver nanoparticles. Appl Clay Sci 97-98:174-181.
30. Rhim JW (2013) Effect of PLA lamination on performance characteristics of agar/κ-carrageenan/clay bio-nanocomposite film. Food Res Int 51:714-722.
31. Tippabattini J, Gownolla MR, KokkaracheduV, Rotimi S, Koduri R, Konduru MR (2013) Iota-Carrageenan-based biodegradable Ag nanocomposite hydrogels for the inactivation of bacteria. Carbohydr Polym 95:188-194.
32. Xudong Z, Dongwei G, Jiquan X, Stavros Y, Ioanna M (2017) The effect of salt concentration on swelling power, rheological properties and saltiness perception of waxy, normal and high amylose maize starch. Food Funct 8:3792.
33. Yoldas S, Aylin A, Basak D, Caner T (2014) Carboxymethylcellulose (CMC)–hydroxyethylcellulose (HEC) based hydrogels: synthesis and characterization. Cellulose 21:1689–1698.
34. Yunpeng L, Yan Q, Ruyu B, Xin Z, Limin Y, Jun L (2019) Preparation of pH-sensitive and antioxidant packaging films based on κ-carrageenan and mulberry polyphenolic extract. Int J Biol Macromol 134:993-1001.
35. Zhili Z, Rendang Y (2017) Novel Nanocomposites Based on Hydroxyethyl Cellulose and Graphene Oxide. Fiber Polym 18:334-341.
36. Zineb K, Faissal A, Hassan H, Hicham BY, Mounir EA (2019) Improved mechanical properties of *k*-carrageenan-based nanocomposite films reinforced with cellulose nanocrystals. Int J Biol Macromol 123:1248-1256.

Figures

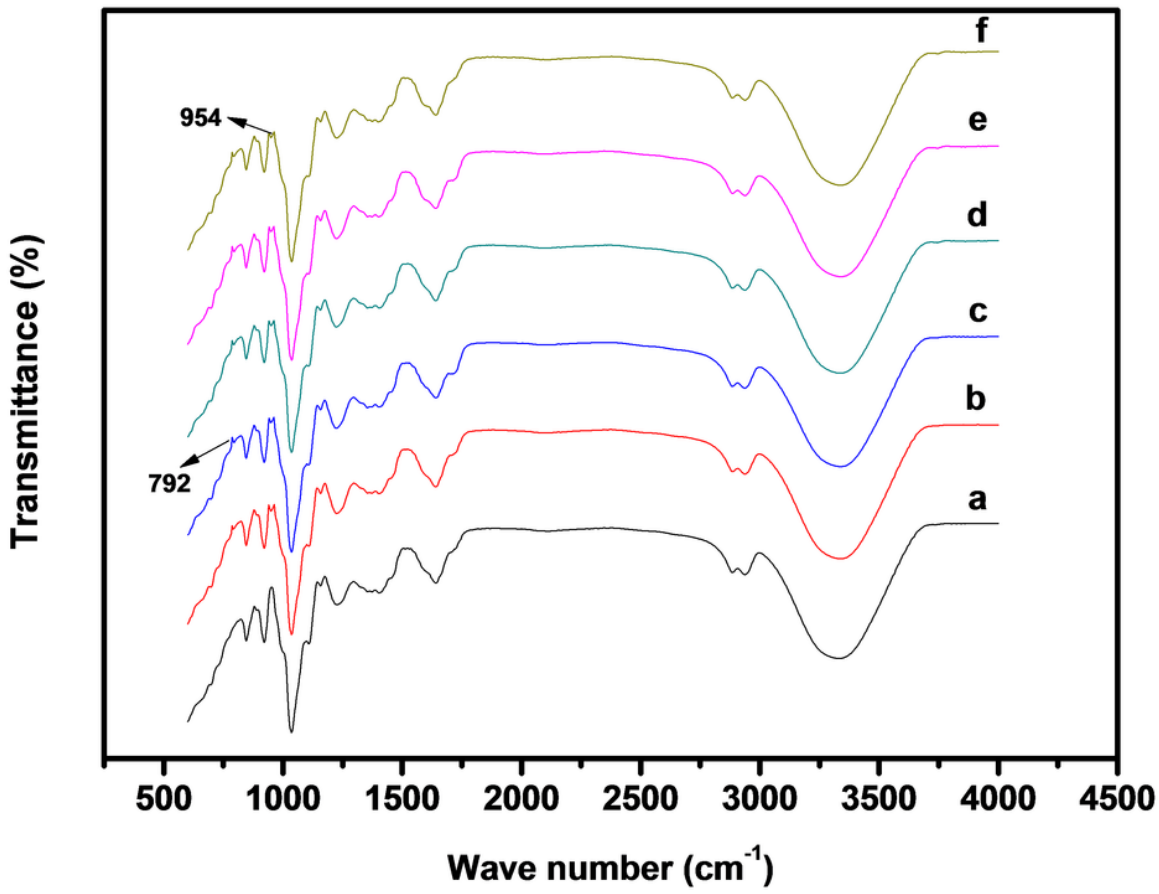

Figure 1

FT-IR spectra of (a) CH (b) CH-SiO2-2.5 wt% (c) CH-SiO2-5 wt % (d) CH-SiO2-7.5 wt% (e) CH-SiO2-10 wt% (f) CH-SiO2-10 wt% /Ag.

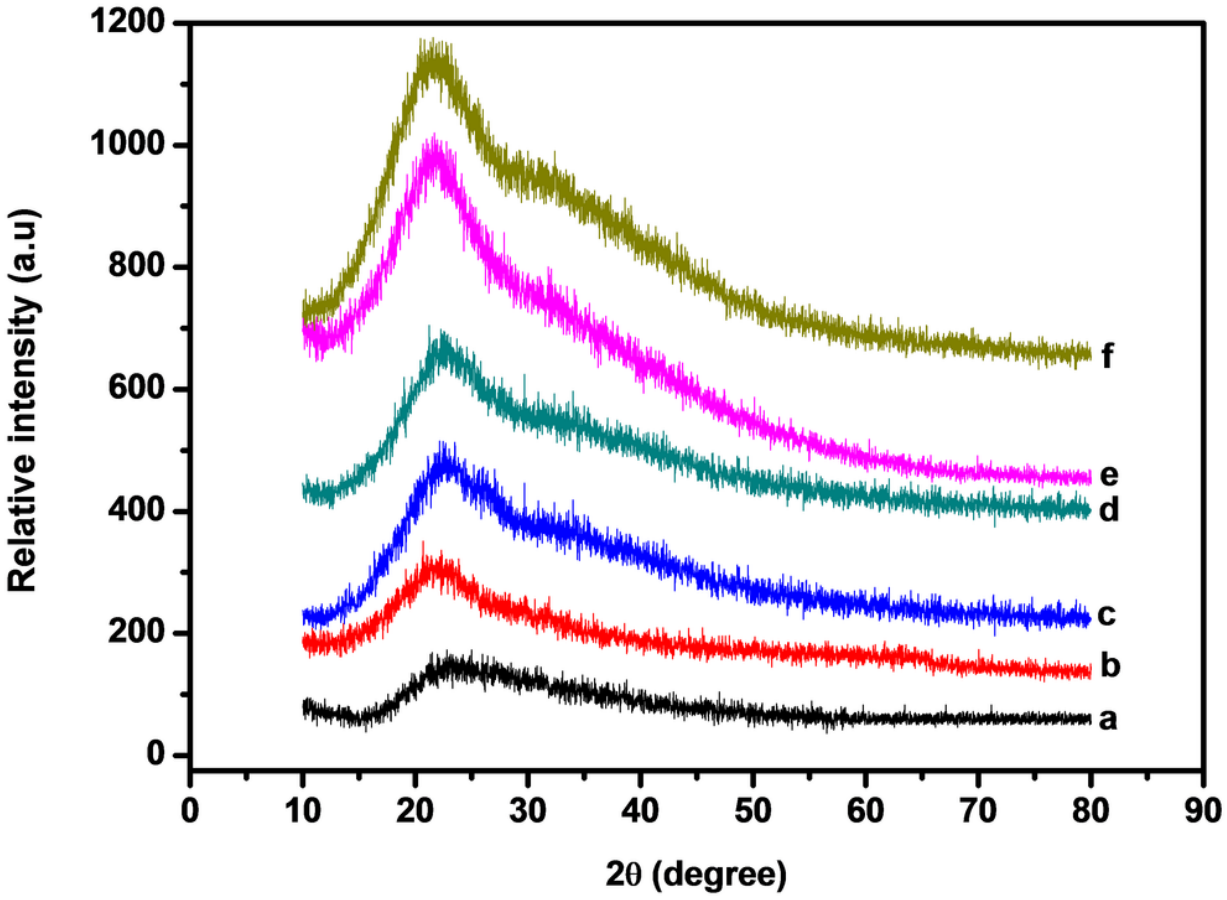

Figure 2

XRD of (a) CH (b) CH-SiO2-2.5 wt% (c) CH-SiO2-5 wt % (d) CH-SiO2-7.5 wt% (e) CH-SiO2-10 wt% (f) CH-SiO¬2-10 wt% /Ag.

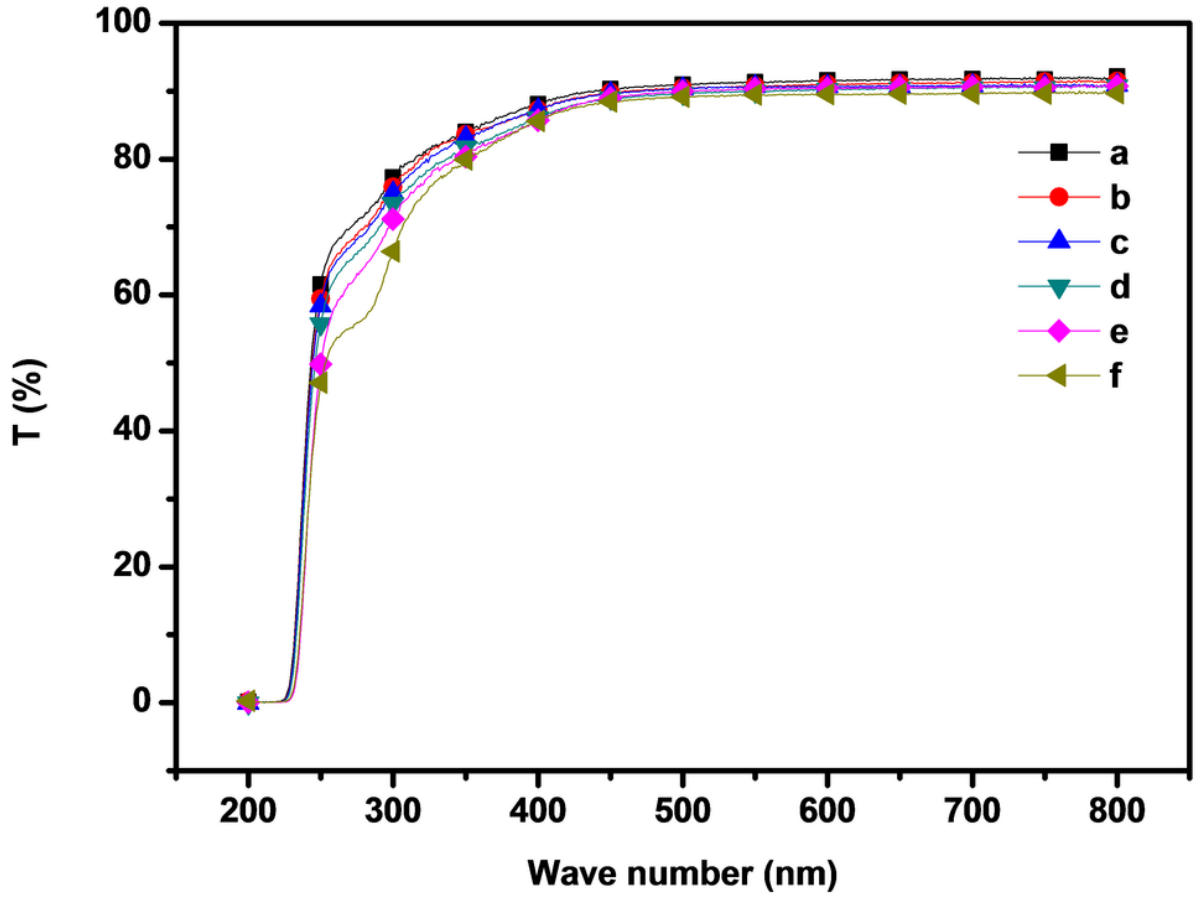

Figure 3

UV transmittance of (a) CH (b) CH-SiO2-2.5 wt% (c) CH-SiO2-5 wt % (d) CH-SiO2-7.5 wt% (e) CH-SiO2-10 wt% (f) CH-SiO2-10 wt% /Ag.

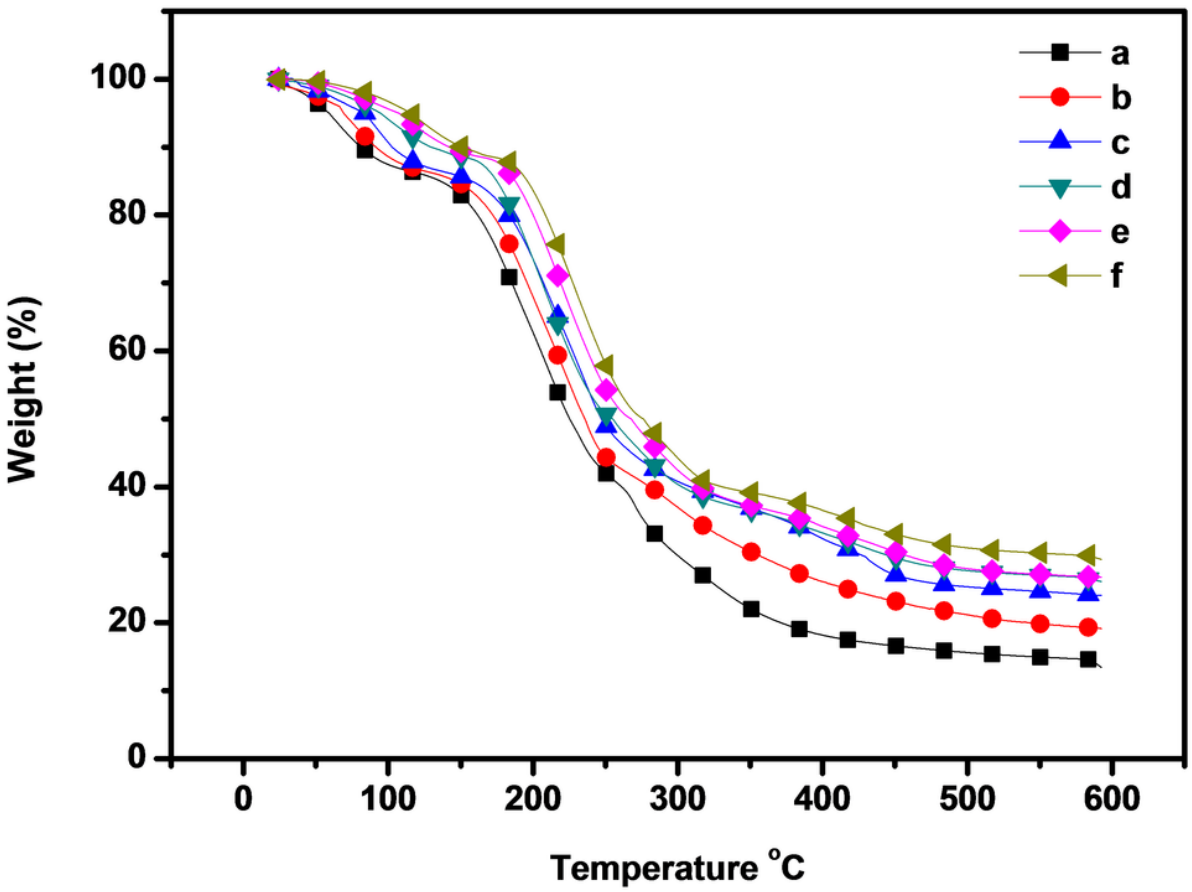

Figure 4

TGA of (a) CH (b) CH-SiO2-2.5 wt% (c) CH-SiO2-5 wt % (d) CH-SiO2-7.5 wt% (e) CH-SiO2-10 wt% (f) CH-SiO2-10 wt% /Ag.

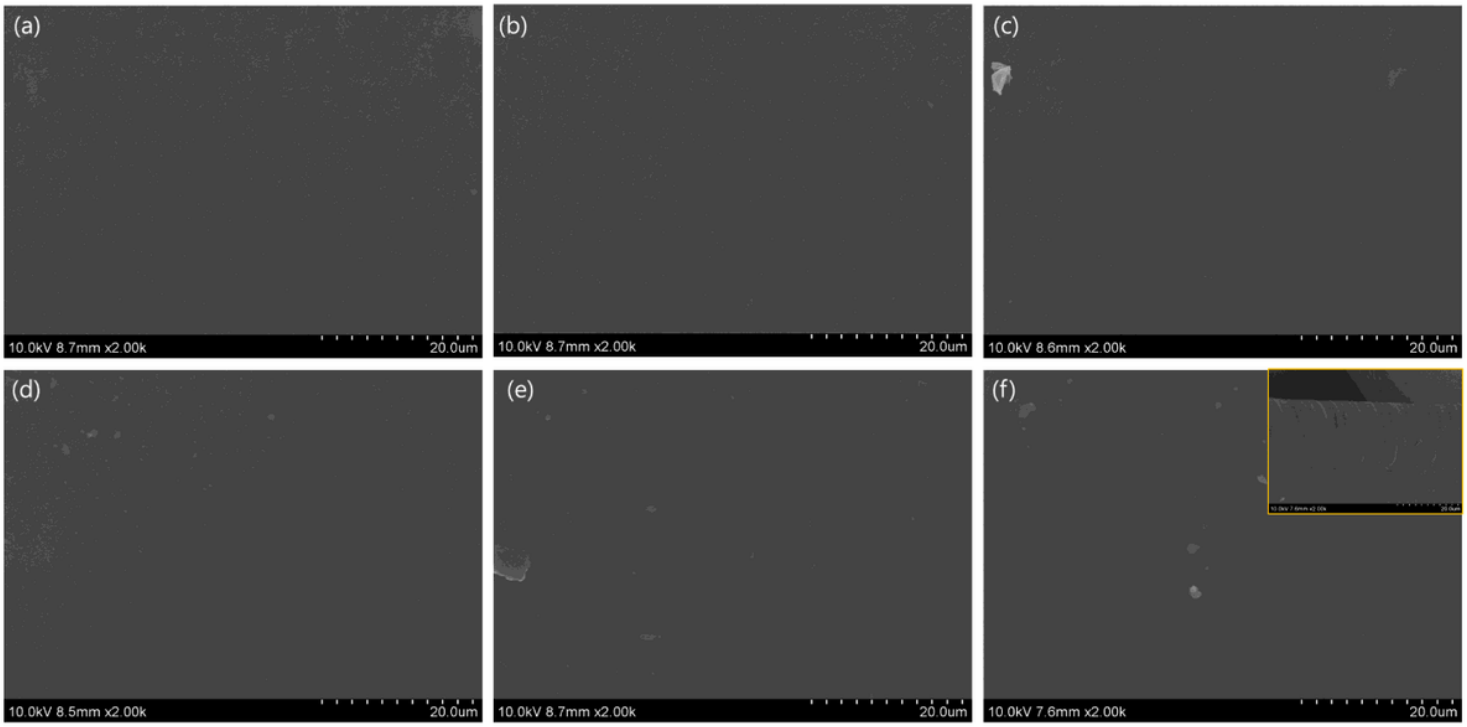

Figure 5

SEM image of (a) CH (b) CH-SiO2-2.5 wt% (c) CH-SiO2-5 wt % (d) CH-SiO2-7.5 wt% (e) CH-SiO2-10 wt% (f) CH-SiO2-10 wt% /Ag.

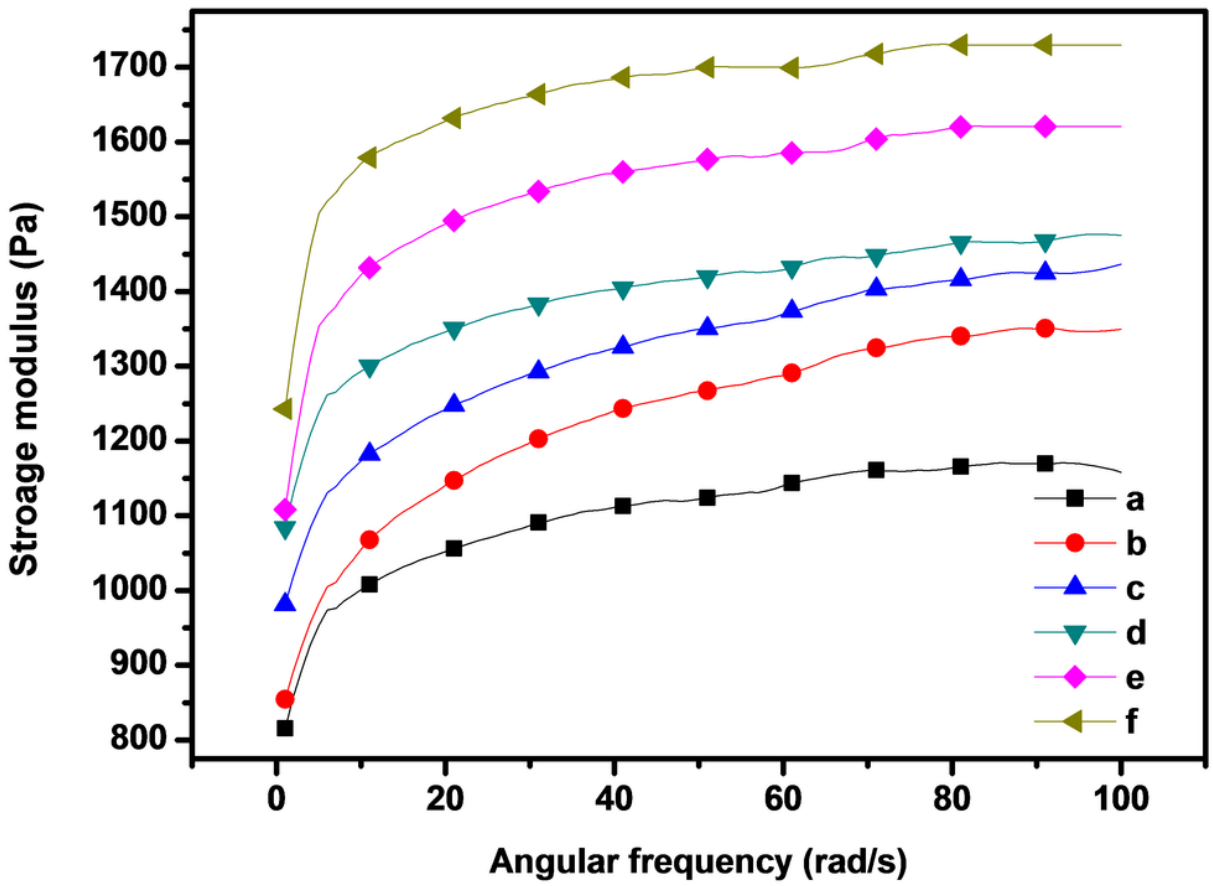

Figure 6

Storage modulus of (a) CH (b) CH-SiO2-2.5 wt% (c) CH-SiO2-5 wt % (d) CH-SiO2-7.5 wt% (e) CH-SiO2-10 wt% (f) CH-SiO2-10 wt% /Ag.

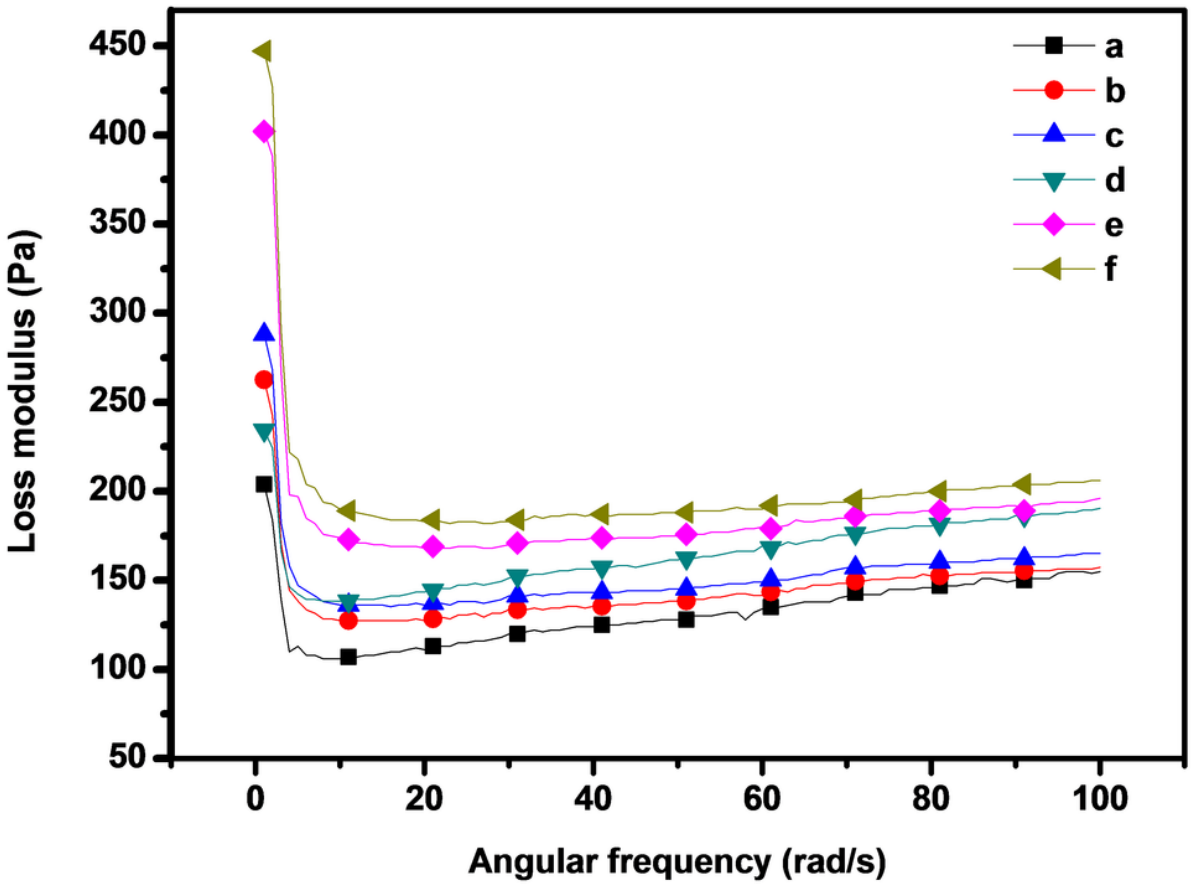

Figure 7

Loss modulus of (a) CH (b) CH-SiO2-2.5 wt% (c) CH-SiO2-5 wt % (d) CH-SiO2-7.5 wt% (e) CH-SiO2-10 wt% (f) CH-SiO2-10 wt% /Ag.

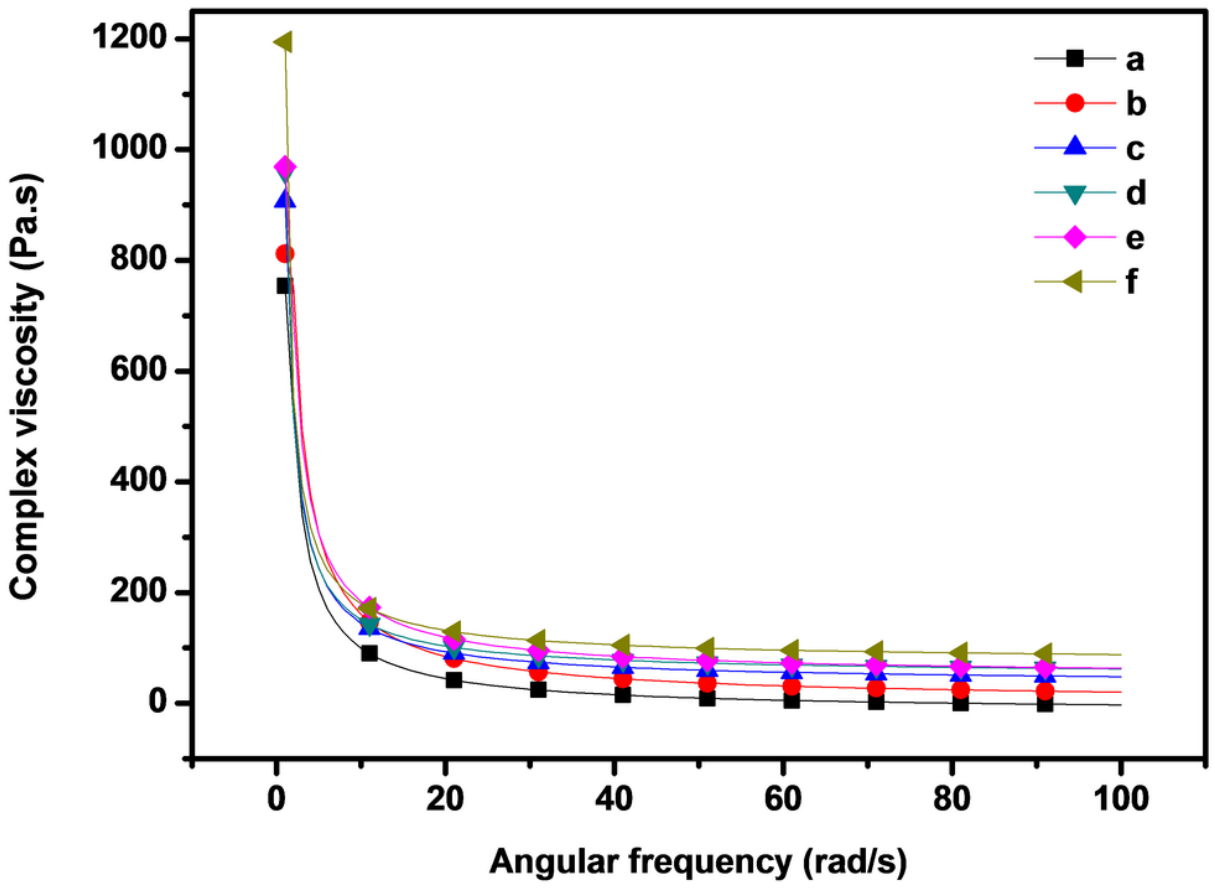

Figure 8

Complex viscosity of (a) CH (b) CH-SiO2-2.5 wt% (c) CH-SiO2-5 wt % (d) CH-SiO2-7.5 wt% (e) CH-SiO2-10 wt% (f) CH-SiO2-10 wt% /Ag.

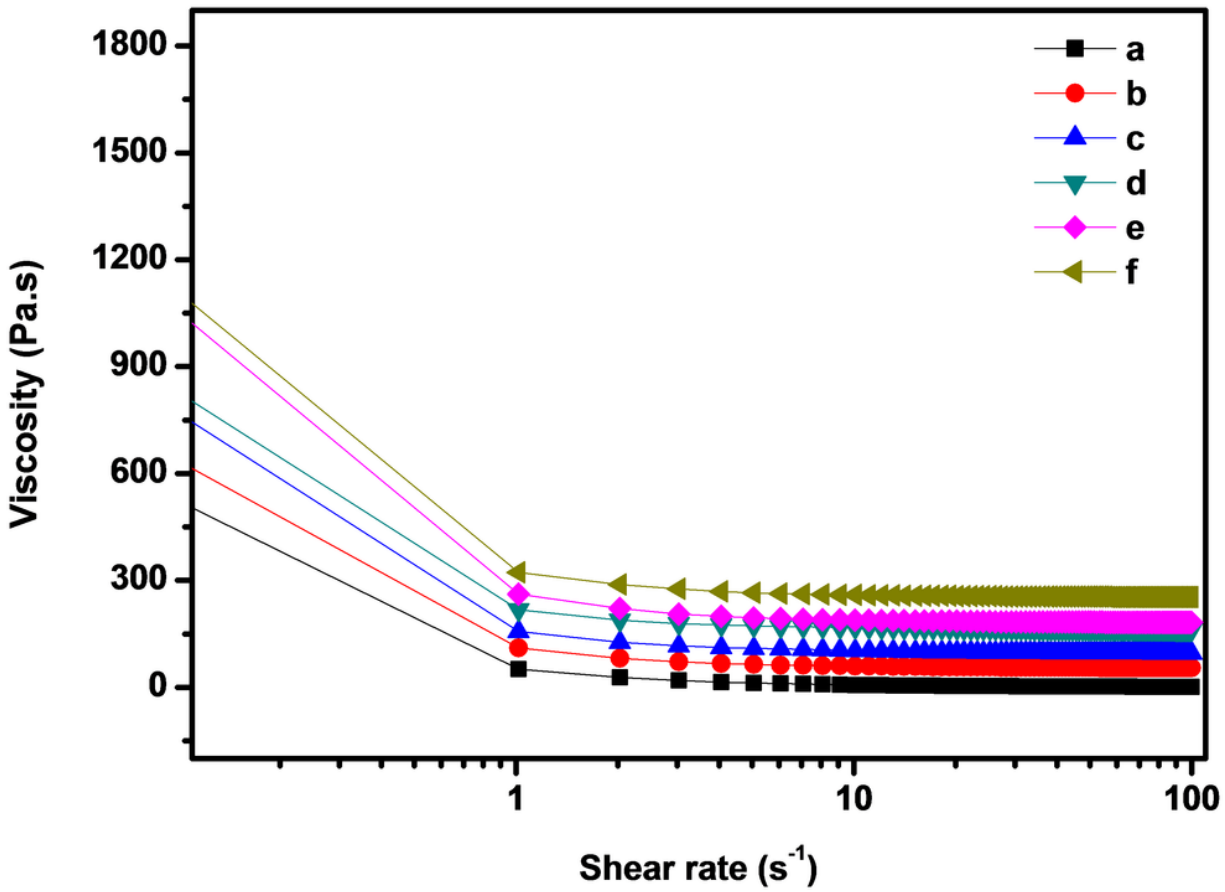

Figure 9

Viscosity of (a) CH (b) CH-SiO2-2.5 wt% (c) CH-SiO2-5 wt % (d) CH-SiO2-7.5 wt% (e) CH-SiO2-10 wt% (f) CH-SiO2-10 wt% /Ag.

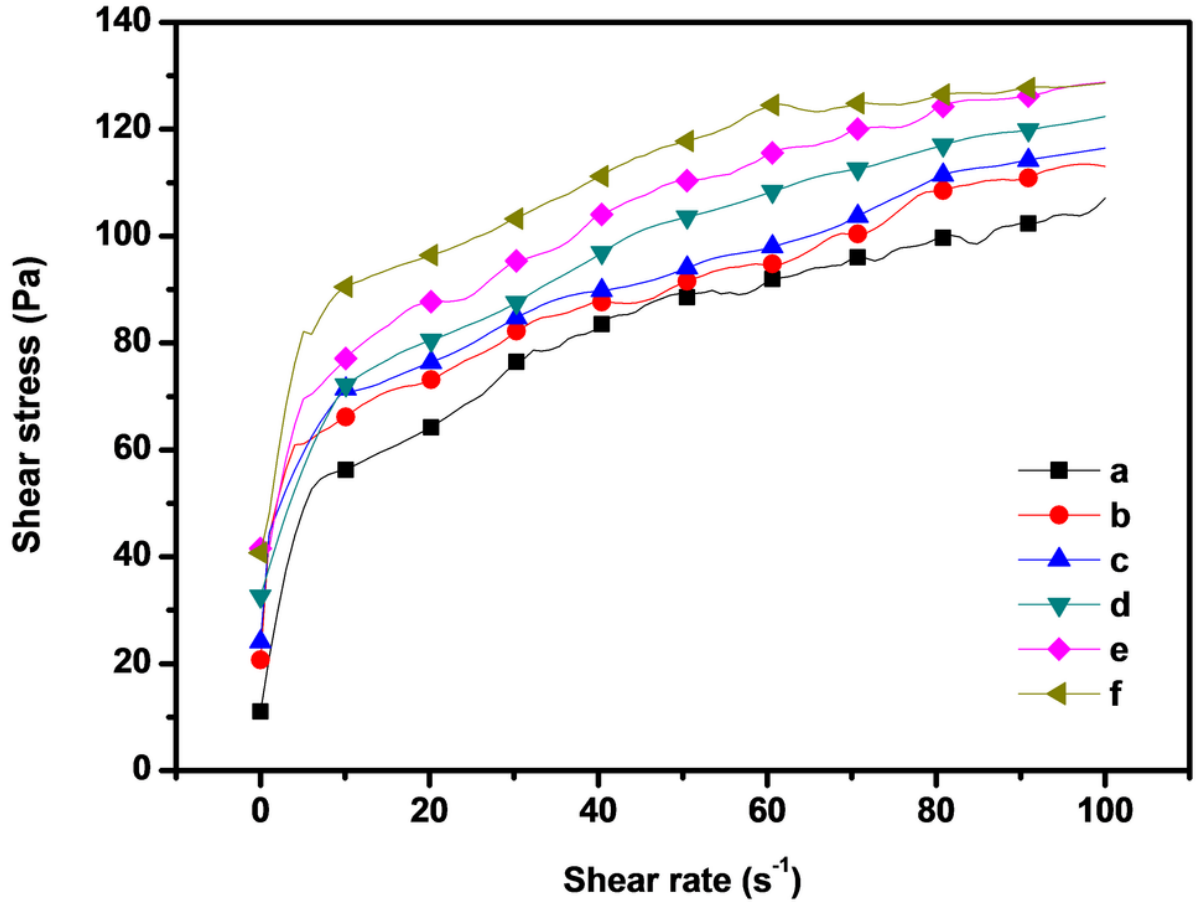

Figure 10

Shear stress versus shear rate of (a) CH (b) CH-SiO2-2.5 wt% (c) CH-SiO2-5 wt % (d) CH-SiO2-7.5 wt% (e) CH-SiO2-10 wt% (f) CH-SiO2-10 wt% /Ag.

Supplementary Files

This is a list of supplementary files associated with this preprint. Click to download.

- Supplementary.docx